# HOKKAIDO UNIVERSITY

| | |
|---|---|
| Title | Role of hierarchy structure on the mechanical adaptation of self-healing hydrogels under cyclic stretching |
| Author(s) | Li, Xueyu; Cui, Kunpeng; Zheng, Yong et al. |
| Citation | Science Advances, 9(51), adj6856<br>https://doi.org/10.1126/sciadv.adj6856 |
| Issue Date | 2023-12-20 |
| Doc URL | https://hdl.handle.net/2115/91367 |
| Type | journal article |
| File Information | ScienceAdvances(2023)_Xueyu_si.pdf |

# Supplementary Materials for

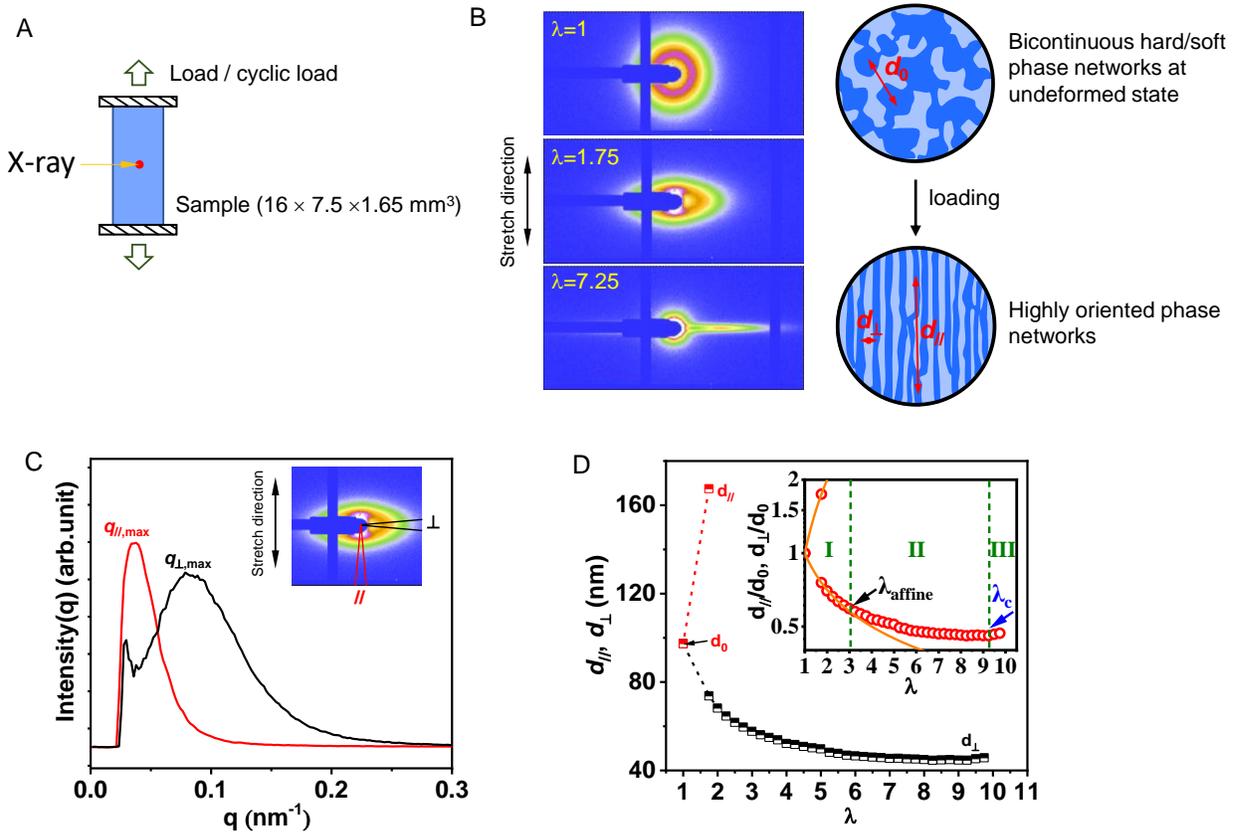## Role of hierarchy structure on the mechanical adaptation of self-healing hydrogels under cyclic stretching

Xueyu Li *et al.*

Corresponding author: Jian Ping Gong, gong@sci.hokudai.ac.jp

**This PDF file includes:**

Figs. S1 to S16
Sections S1 to S4
Table S1
References

**Fig. S1. Bicontinuous phase separation structure of s-PA and its deformation under loading characterized by *in-situ* SAXS. (A)** The illustration of the specimen used in *in-situ* SAXS tests. The rectangular sample ($L_0$ = 7.5 mm, $H_0$ = 16 mm, thickness 1.65 mm) was used. The loading strain rate is 1 $s^{-1}$. **(B)** Typical 2D SAXS patterns under the uniaxial tensile ($\lambda$ = 1, 1.75, 7.25 are taken as examples). We can see from the patterns, with increasing stretch ratio $\lambda$, the phase networks become oriented along the stretching direction (schemed in the right figure). **(C)** 1D scattering profiles $I(q)$ as a function of $q$ at $\lambda$ = 1.75 in parallel (//) and perpendicular ($\perp$) to the stretch direction. Inset shows the sector regions for integrating the 1D scattering intensity. From the position of scattering peaks ($q_{//,max}$ and $q_{\perp,max}$), we obtain the $d$-spacing change in the stretching direction ($d_{//}$) and perpendicular direction ($d_\perp$), by $d_{//} = 2\pi/q_{//,max}$ and $d_\perp = 2\pi/q_{\perp,max}$, respectively. **(D)** The $d_{//}$ and $d_\perp$ as a function of $\lambda$. The $d$-spacing ($d_0$) between adjacent soft regions or hard regions in the undeformed gel is $d_0 \approx 100$ nm. When the gel is loaded to $\lambda > 1.75$, the $d_{//}$ exceeds the detecting range. The microscopic deformation is obtained by $d_{//}/d_0$ and $d_\perp/d_0$. Inset shows the $d_{//}/d_0$ and $d_\perp/d_0$ as a function of the macroscopic stretch ratio $\lambda$. The orange lines stand for the prediction of affine deformation of the phase networks (for incompressible materials, the affine deformation follows $d_{//}/d_0 = \lambda$ and $d_\perp/d_0 = \lambda^{-1/2}$). The data is extracted from ref (*49*). The $d_\perp/d_0$ versus $\lambda$ curve can be divided into three regimes with the split points $\lambda_{affine}$ (black arrow) and $\lambda_c$ (blue arrow). The $\lambda_{affine}$ ($\lambda_{affine}$ = 3.06) is determined by the critical point at which the microscopic deformation of the phase network begins to deviate from the predicted affine deformation. The $\lambda_c$ ($\lambda_c$ = 9.2) is determined by the point at which $d_\perp/d_0$ slightly increases with $\lambda$. According to our previous work (*51*), the percolated hard and soft phase networks deform equally at stretch ratio $\lambda < \lambda_{affine}$ (regime I), but the hard phase network sustains more stress due to high stiffness. At $\lambda = \lambda_{affine}$, damage to the hard phase strands begins to occur as they carry most of the stress, and the contraction of the damaged hard phase strands exerts a large shear stress on the adjacent soft phase

strands. The load is transferred to adjacent hard-phase strands via the soft-phase strands (regime II). With increasing $\lambda$, more hard phase strands rupture until the shear stress is larger than the strength of the soft phase strands, resulting in the soft phase network rupture at $\lambda = \lambda_c$. The rupture of the soft phase network results in a catastrophic fracture of the whole sample immediately (regime III). Above the $\lambda = \lambda_c$, the $d_\perp/d_0$ increases with $\lambda$ since the rupture of soft phase strands destroys the ordering of neighboring hard phase strands. Therefore, the $\lambda_{\text{affine}}$ denotes the onset of damage to the hard-phase network, and the $\lambda_c$ denotes the onset of damage to the soft-phase network.
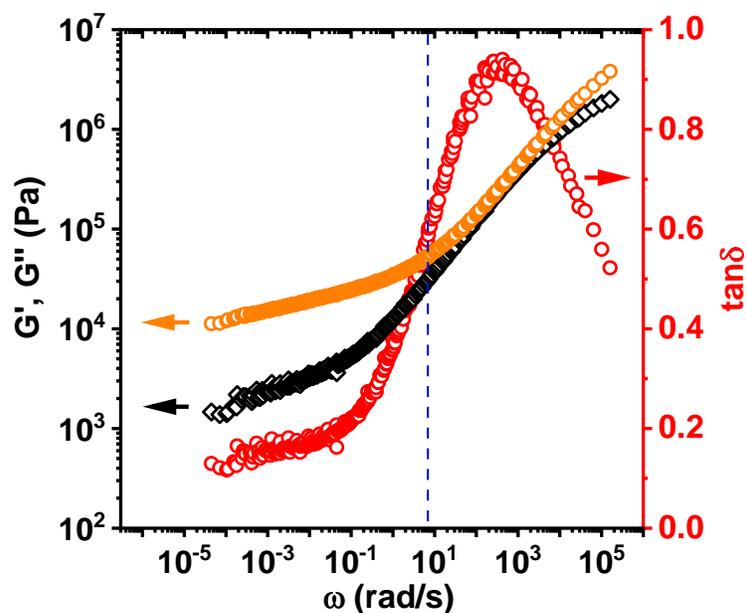
**Fig. S2. Dynamic mechanical behavior of the s-PA gel.** Frequency ($\omega$) dependence of the storage modulus $G'$, loss modulus $G''$, and loss factor tan$\delta$. The vertical dotted line indicates the angular frequency at $\omega = 2\pi\dot{\varepsilon}$ (45) for the strain rate of cyclic loading $\dot{\varepsilon} = 1\ \text{s}^{-1}$. $G'$ does not reach the plateau modulus at the high frequency limit, indicating that the lifetime of ionic bonds ($\tau_s$) is short, beyond our observation window ($\tau_s < 10^{-5}\ \text{s}$). The data is adopted from ref (47).

## Section S1. Cyclic training behaviors of soft materials with or without hierarchical structure

To illustrate the effect of the hierarchical structure in cyclic training, we subjected two control samples to cyclic loading (stretching): one with very weak phase separation (w-PA gel) and another without phase separation but with good self-healing properties (PPEA elastomer).
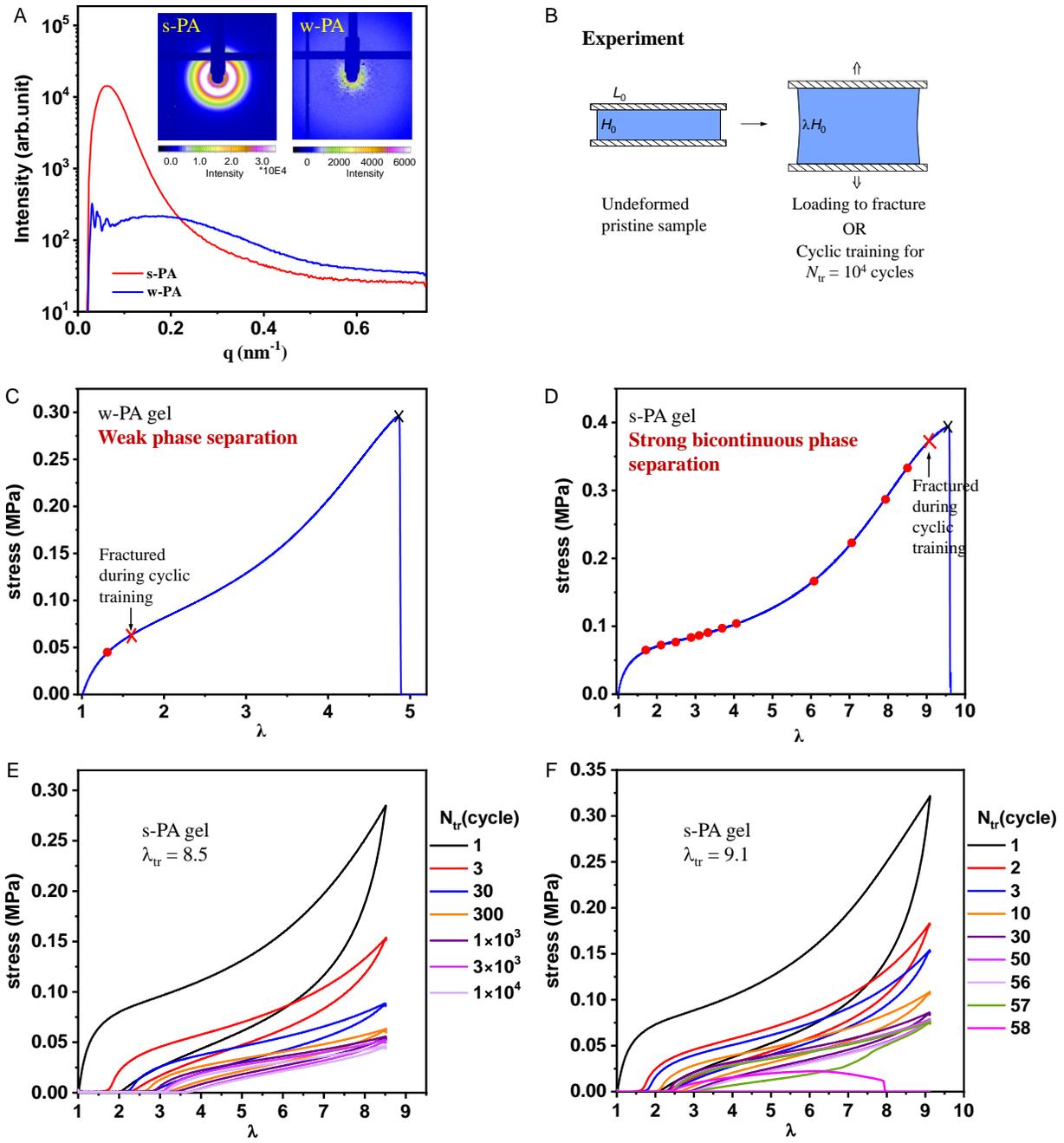


**Fig. S3. Comparison of fracture behavior in strong (s-PA) and weak (w-PA) phase-separated PA gels under monotonic and cyclic stretching.** (**A**) SAXS result for s-PA and w-PA. s-PA
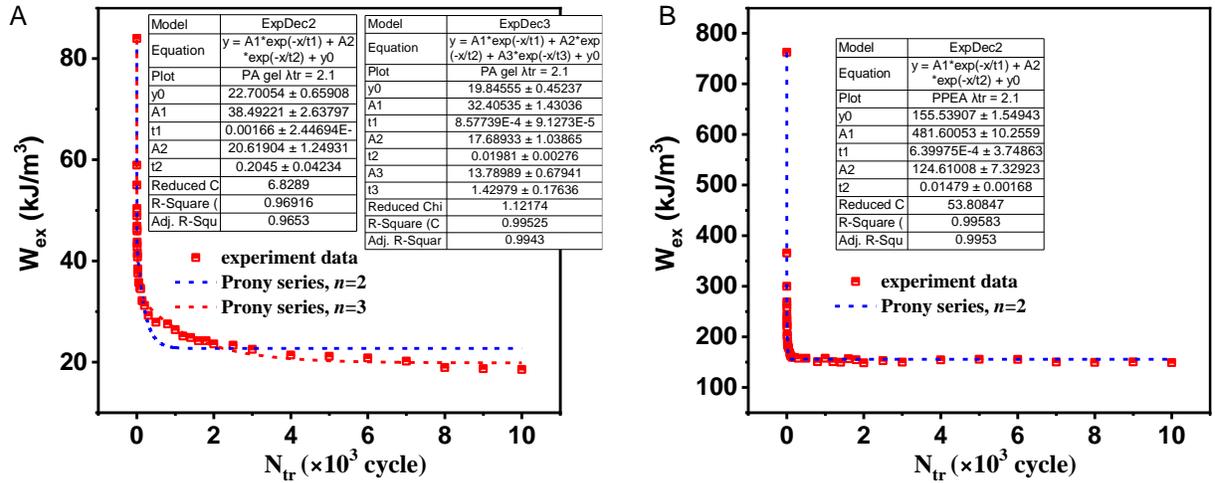
exhibits a pronounced density contrast (proportional to the modulus contrast) tween its hard and soft phase domains, while w-PA displays a substantially weak density contrast between the two phases. (**B**) Pure shear geometry used for monotonic and cyclic stretching ($L_0 = 50$ mm, and $H_0 = 10$ mm). (**C**) The stress-stretch (S-S) curve for w-PA gel. (**D**) The S-S curve for s-PA gel. In figure C and D, the black "X" denotes sample fracture under monotonic stretching. The red "X" indicates sample fracture under cyclic stretching condition. The red dots denote the sample capable of enduring $N_{tr} = 10^4$ cycles at $\lambda_{tr}$ equal to the corresponding $\lambda$ without fracture. (**E**) Evolution of loading-unloading curves with training cycle ($N_{tr}$) at $\lambda_{tr} = 8.5$ for s-PA. (**F**) Evolution of loading-unloading curves with training cycle ($N_{tr}$) at $\lambda_{tr} = 9.1$ for s-PA.
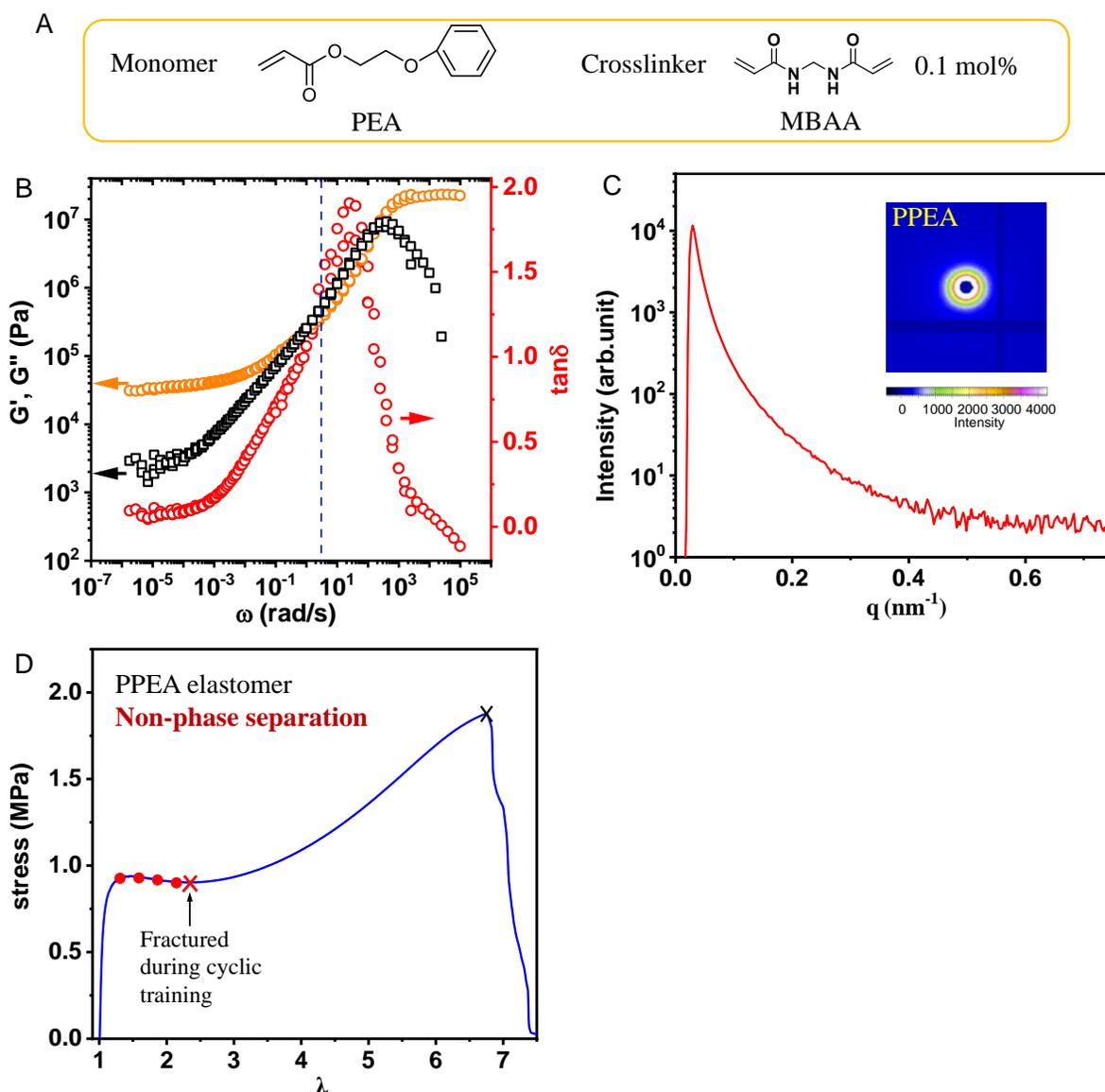
**Fig. S4. Dynamic mechanical behavior, SAXS result, and cyclic training behavior of the PPEA elastomer.** (**A**) Chemical structure of ethylene glycol phenyl ether acrylate (PEA) monomer. The PPEA elastomer is crosslinked by 0.1 mol% MBAA in relative to the monomer. (**B**) Frequency ($\omega$) dependence of the storage modulus $G'$, loss modulus $G''$, and loss factor $\tan\delta$. The vertical dotted line indicates the angular frequency at $\omega = 2\pi\dot{\varepsilon}$ for the strain rate of cyclic loading $\dot{\varepsilon} = 0.5$ $s^{-1}$. (**C**) SAXS result. The SAXS result shows no phase separation and the WAXS result shows no crystallization in the PPEA elastomer (*55*). These results suggest that no hierarchical structure formed in PPEA elastomer. (**D**) The S-S curve for PPEA elastomer. The black "X" denotes sample fracture under monotonic stretching. The red "X" indicates sample fracture under cyclic stretching condition. The red dots denote the sample capable of enduring $N_{tr} = 10^4$ cycles at $\lambda_{tr}$ equal to the corresponding $\lambda$ without fracture.
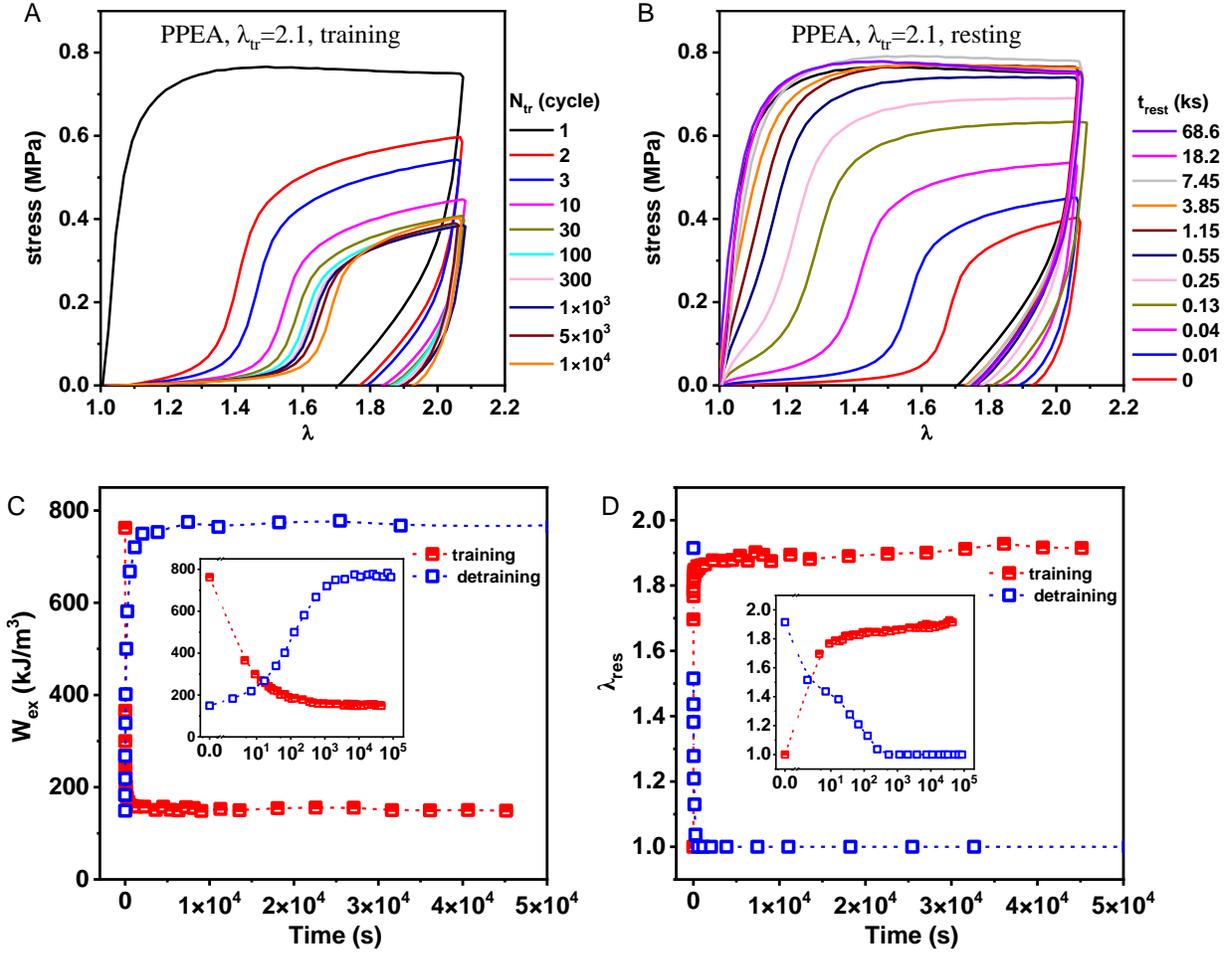
**Fig. S5. Cyclic training of PPEA elastomer.** The same pure shear geometry as **Fig. 2A** was used for the training. Training was performed at 24 °C with an initial strain rate $\dot{\varepsilon} = 0.5 \text{ s}^{-1}$. (**A**) Evolution of loading-unloading curves with training cycle ($N_{tr}$). (**B**) Loading-unloading curves for a trained gel resting for $t_{rest}$. (**C**) $W_{ex}$ as a function of time (red: training, blue: detraining). (**D**) $\lambda_{res}$ as a function of time (red: training, blue: detraining). Training at $\lambda_{tr} = 2.1$ for $N_{tr} = 10^4$ cycles is taken as an example. We can observe that the training curves reach the steady state rapidly, and both the $W_{ex}$ and $\lambda_{res}$ fully recover quickly during detraining. This suggests that the PPEA elastomer does not possess a long-term memory of the training effect.

**A**

| Model | ExpDec2 |
|---|---|
| Equation | y = A1*exp(-x/t1) + A2*exp(-x/t2) + y0 |
| Plot | PA gel λtr = 2.1 |
| y0 | 22.70054 ± 0.65908 |
| A1 | 38.49221 ± 2.63797 |
| t1 | 0.00166 ± 2.44694E- |
| A2 | 20.61904 ± 1.24931 |
| t2 | 0.2045 ± 0.04234 |
| Reduced C | 6.8289 |
| R-Square ( | 0.96916 |
| Adj. R-Squ | 0.9653 |

| Model | ExpDec3 |
|---|---|
| Equation | y = A1*exp(-x/t1) + A2*exp(-x/t2) + A3*exp(-x/t3) + y0 |
| Plot | PA gel λtr = 2.1 |
| y0 | 19.84555 ± 0.45237 |
| A1 | 32.40535 ± 1.43036 |
| t1 | 8.57739E-4 ± 9.1273E-5 |
| A2 | 17.68933 ± 1.03865 |
| t2 | 0.01981 ± 0.00276 |
| A3 | 13.78989 ± 0.67941 |
| t3 | 1.42979 ± 0.17636 |
| Reduced Chi | 1.12174 |
| R-Square (C | 0.99525 |
| Adj. R-Squar | 0.9943 |

- ■ experiment data
- - - - Prony series, $n=2$
- - - - Prony series, $n=3$

**B**

| Model | ExpDec2 |
|---|---|
| Equation | y = A1*exp(-x/t1) + A2*exp(-x/t2) + y0 |
| Plot | PPEA λtr = 2.1 |
| y0 | 155.53907 ± 1.54943 |
| A1 | 481.60053 ± 10.2559 |
| t1 | 6.39975E-4 ± 3.74863 |
| A2 | 124.61008 ± 7.32923 |
| t2 | 0.01479 ± 0.00168 |
| Reduced C | 53.80847 |
| R-Square ( | 0.99583 |
| Adj. R-Squ | 0.9953 |

- ■ experiment data
- - - - Prony series, $n=2$

**Fig. S6. Prony series fitting for $W_{ex}$ versus $N_{tr}$ curve of s-PA hydrogel and PPEA elastomer trained at $\lambda_{tr} = 2.1$ and $N_{tr} = 10^4$ cycles.** (**A**) Comparison of the fitting curve by the two-term ($n = 2$) and three-term ($n = 3$) Prony series fitting of s-PA hydrogel. (**B**) Two-term ($n = 2$) Prony series fitting for PPEA elastomer. The fitting equation is $y = y_0 + \sum_{i=1}^{n} A_i e^{-x/t_i}$, where $y$ corresponds to $W_{ex}$, $x$ is $N_{tr}$, $t_i$ is the characteristic training cycles $N_i$, and $y_0$ is the equilibrium $W_{ex}$ of the cyclic training. From the fitting we obtained training cycle parameters $N_1(\sim0.6)$ and $N_2(\sim15)$ for $W_{ex}$ of the PPEA.

**Table S1. The comparison of training time and full recovery time of s-PA gel and PPEA elastomer.**

| Material | $\lambda_{tr}$ | Total training time | Full recovery time for $W_{ex}$[a] | Full recovery time for $\lambda_{res}$[b] |
|---|---|---|---|---|
| PPEA elastomer | 1.3 | 14.2 ks | 1147 s | 67 s |
| PPEA elastomer | 1.8 | 35.2 ks | 3847 s | 547 s |
| PPEA elastomer | 2.1 | 45.1 ks | 7447 s | 547 s |
| s-PA gel | 1.3 | 8.7 ks | 18247 s | 7447 s |
| s-PA gel | 1.7 | 17.8 ks | 68647 s | 18247 s |
| s-PA gel | 2.1 | 26.1 ks | >86647 s | 18247 s |

[a] Full recovery time for $W_{ex}$ represents the time it took for $W_{ex}(t_{rest})$ to recover to $W_{ex0}$ which was the work of extension of the first loading to corresponding $\lambda_{tr}$. [b] Full recovery time for $\lambda_{res}(t_{rest})$ represents the time it took for $\lambda_{res}(t_{rest})$ to recover to a value of 1.

## Section S2. The Prony series fitting of training curves

The $W_{ex}$ and $\lambda_{res}$ in training process are obtained from the loading-unloading curves as shown in **Fig. 2** (**B, C** and **D**). **Fig. S7B** shows that $W_{ex}$ and $\lambda_{res}$ change rapidly at the beginning training cycles and then reach the plateau. This is universal for training at varied $\lambda_{tr}$. As shown in **fig. S7C**, all the normalized $W_{ex}/W_{ex0}$ ($W_{ex0}$ is the work of extension of the first loading to corresponding $\lambda_{tr}$) versus $N_{tr}$ curves exhibit similar behavior, that the required energy to deform the gel to a certain stretch ratio ($\lambda_{tr}$) decreases with training cycle and finally almost reaches saturation.

To elucidate the contribution of the hierarchy structure to training process, we use the generalized Maxwell model (Prony series) to analyze the plot of $W_{ex}$ versus $N_{tr}$. The Prony series consists of a spring and $n$ Maxwell elements connected in parallel (*68, 69*), which is a phenomenological model commonly used to fit the relaxation dynamics of viscoelastic material such as biological tissues (*70*), elastomers (*69, 71*), hydrogels (*72, 73*), etc. Here, we try to use the Prony series to fit the reduction of energy required for a preset $\lambda_{tr}$ during training, we rewrite the Prony series as

$$W(N_{tr}) = W_{\infty} + \sum_{i=1}^{n} W_i e^{-N_{tr}/N_i} \tag{S1}$$

where $W(N_{tr})$ is the $W_{ex}$ at the $N_{tr}$, $W_{\infty}$ is the equilibrium $W_{ex}$ of the cyclic training, $N_i$ are the characteristic training cycles, $W_i$ are training strengths correlated to the reduction of $W_{ex}$, and $n$ is the series order. We find that $n = 3$ were sufficient to fit the $W_{ex}$ versus $N_{tr}$ curves (**fig. S6A**). **Fig. S7D** shows an example of the fitting result at $\lambda_{tr} = 2.9$ and total $N_{tr} = 10^4$ cycles. From the fitting results, we obtain three characteristic training cycles $N_1 = 1$ cycle, $N_2 = 18$ cycle, $N_3 = 1003$ cycle, with the training strengths $W_1 = 49.3$ kJ/m$^3$, $W_2 = 29.8$ kJ/m$^3$, $W_3 = 19$ kJ/m$^3$, and $W_{\infty} = 31.1$ kJ/m$^3$.

The Prony series fitting parameters of gel training at varied $\lambda_{tr}$ for $N_{tr} = 10^4$ cycles are presented in **fig. S7E** and the normalized $W_i/W_{ex0}$ and $W_{\infty}/W_{ex0}$ are shown in **fig. S7F**. The characteristic training cycles $N_1(\sim 1)$, $N_2(\sim 20)$, $N_3(\sim 1000)$ are shown in **Fig. 3A**. By comparing the characteristic

times with the non-phase-separated PPEA and rheological result, we assign $N_1(\sim 1)$, $N_2(\sim 20)$, $N_3(\sim 1000)$ to short scale ionic breaking, the local adaption of transient networks, and the adaption of hard phase network, respectively. The decrease of $W_\infty/W_{ex0}$ and $W_3/W_{ex0}$ at $\lambda_{affine} < \lambda_{tr} < \lambda_c$ support that the broken of hard phase network (with longest characteristic training time) weakens the training effect. The characteristic training times, $\tau_1$, $\tau_2$, $\tau_3$, are obtained from the product of $N_i$ and the corresponding training time per cycle. $\tau_1$, $\tau_2$, $\tau_3$ in three different orders of magnitude increase with $\lambda_{tr}$ (**fig. S7G**). But the slopes of $\tau_i$ versus $\lambda_{tr}$ change around the $\lambda_{affine}$, indicating that the training dynamics are affected by the damage in the hard phase network.
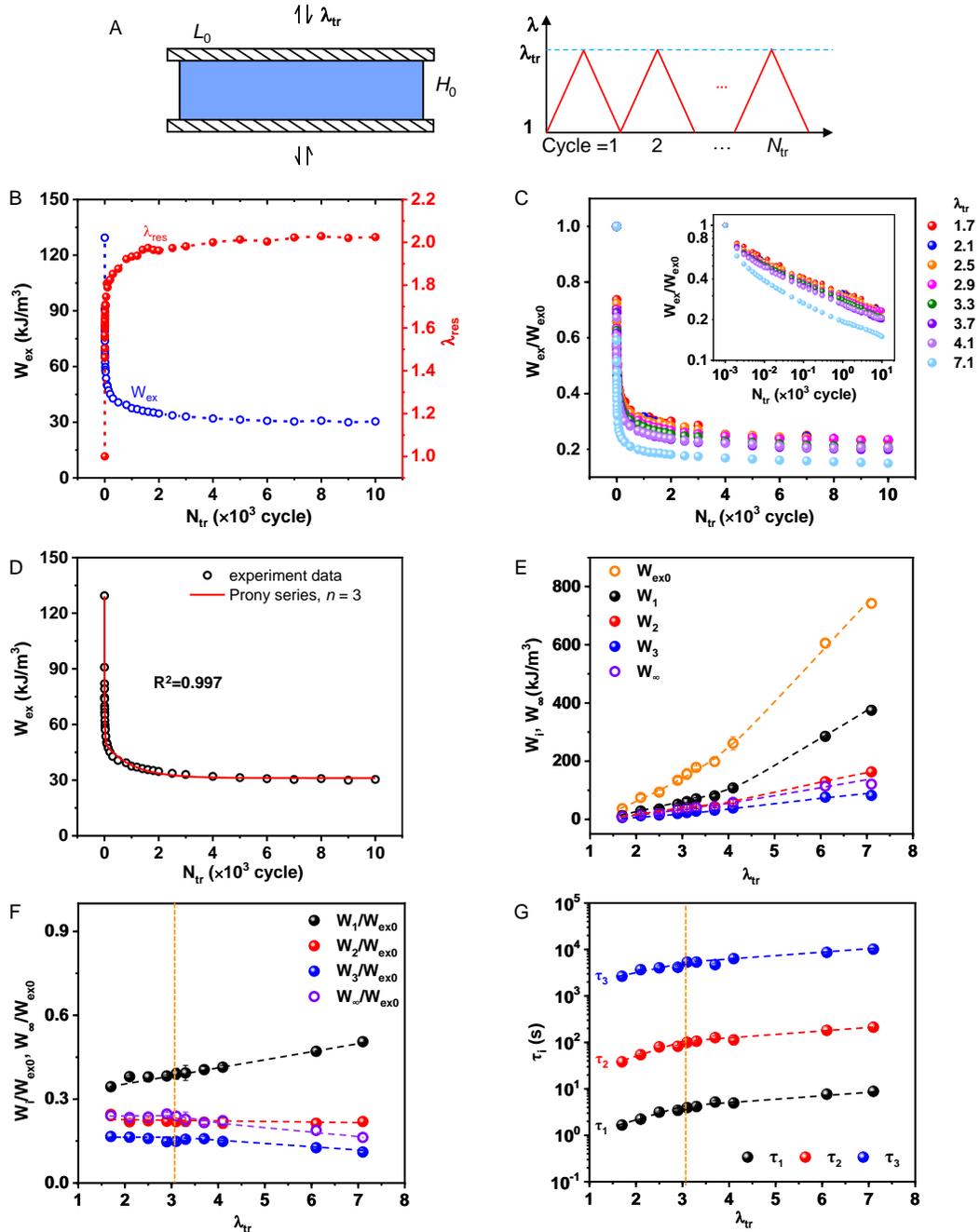
**Fig. S7. Evolution of work of extension ($W_{ex}$) with training cycle $N_{tr}$ of s-PA gel and the Prony series fitting.** (**A**) Pure shear geometry ($L_0 = 50$ mm, $H_0 = 10$ mm) and triangle loading profile for cyclic training. During cyclic training, the maximum and minimum stretch ratios are kept at pre-set values $\lambda_{tr}$ and 1, respectively. (**B**) The $W_{ex}$ and $\lambda_{res}$ as a function of $N_{tr}$. Training at $\lambda_{tr} = 2.9$ is taken as an example. (**C**) Normalized $W_{ex}/W_{ex0}$ versus $N_{tr}$ for the samples tested at varied $\lambda_{tr}$. $W_{ex0}$ is work of extension of the first loading to $\lambda_{tr}$. Inset shows the plots in a logarithmic scale. (**D**) Fitting the $W_{ex}$ versus $N_{tr}$ curve by the Prony series. $\lambda_{tr} = 2.9$ is taken as an example. The number of terms in the Prony series is picked to be $n = 3$. (**E**) The Prony series fitting parameter $W_i$, $W_\infty$ and $W_{ex0}$ as a function of $\lambda_{tr}$. (**F**) Normalized Prony series fitting parameter $W_i/W_{ex0}$ and $W_\infty/W_{ex0}$ as a function of $\lambda_{tr}$. (**G**) The characteristic training times $\tau_1$, $\tau_2$, $\tau_3$ of $W_{ex}$ (product of characteristic training cycles $N_i$ and time consumption per cycle $t_{cycle}$) as a function of $\lambda_{tr}$. The vertical dotted line in **F-G** indicates $\lambda_{affine}$. The dashed lines are a guide for the eyes. The error bar ($\lambda_{tr} = 2.1$ to $3.7$) is standard error (SE) from at least three measurements.

The $\lambda_{res}$ increases sharply with $N_{tr}$ at the beginning of the training and then reach a steady state (**fig. S8A**). To study the dynamics of residual stretch ratio $\lambda_{res}$ during training, we use the Prony series to fit the normalized $\lambda_{res}$ versus $N_{tr}$ curves. The $\lambda_{res}$ is normalized as

$R(N_{tr}) = \dfrac{\lambda_{res}(N_{tr}) - \lambda_{res}(\infty)}{\lambda_{res}(0) - \lambda_{res}(\infty)}$, where $\lambda_{res}(N_{tr})$ is the residual stretch ratio at cycle $N_{tr}$, $\lambda_{res}(\infty)$ is the residual stretch ratio at the steady state of training (**fig. S8B**). $\lambda_{res}(0) = 1$ denotes the $\lambda_{res}$ at undeformed state. The $R(N_{tr})$ denotes the relative training effect away from the steady state. Thus, the Prony series for fitting $R(N_{tr})$ is rewritten as

$$R(N_{tr}) = R_{\infty} + \sum_{i=1}^{n} R_i e^{-N_{tr}/N_i} \tag{S2}$$

Where $R_{\infty}$ is close to 0 since $N_{tr} = 10^4$ already reaches the steady state, $R_i$ are training strengths for $\lambda_{res}$, and $N_i$ are the characteristic training cycles of $\lambda_{res}$. **Fig. S8C** shows an example of the fitting result ($\lambda_{tr} = 2.9$) using $n = 3$. The obtained characteristic training cycles are $N_1 = 1$, $N_2 = 19$, and $N_3 = 962$, with the fitting parameters $R_1 = 0.51$, $R_2 = 0.27$, $R_3 = 0.21$, and $R_{\infty} = 0.01$.

The characteristic training cycles $N_i$ of $\lambda_{res}$ for s-PA gel are shown in **Fig. 3B**, and the corresponding fitting parameters are shown in **fig. S8D**. As expected, the $R_{\infty}$ is close to 0. The training strength of the first term $R_1$, corresponding to $N_1 \approx 1$, has a largest value than others as the first training cycle induces a large $\lambda_{res}$ by breaking the ionic bonds and elongating polymer network. $R_1$ decreases while the second and third term $R_2$, $R_3$ increase slightly with $\lambda_{tr}$ at $\lambda_{tr} < \lambda_{affine}$. This could be correlated to a higher oriented phase networks formed at larger $\lambda_{tr}$, and the contribution from the long-term adaptation increasing. At $\lambda_{affine} < \lambda_{tr} < \lambda_c$, all the parameters almost keep constant due to the damage of the hard phase network.
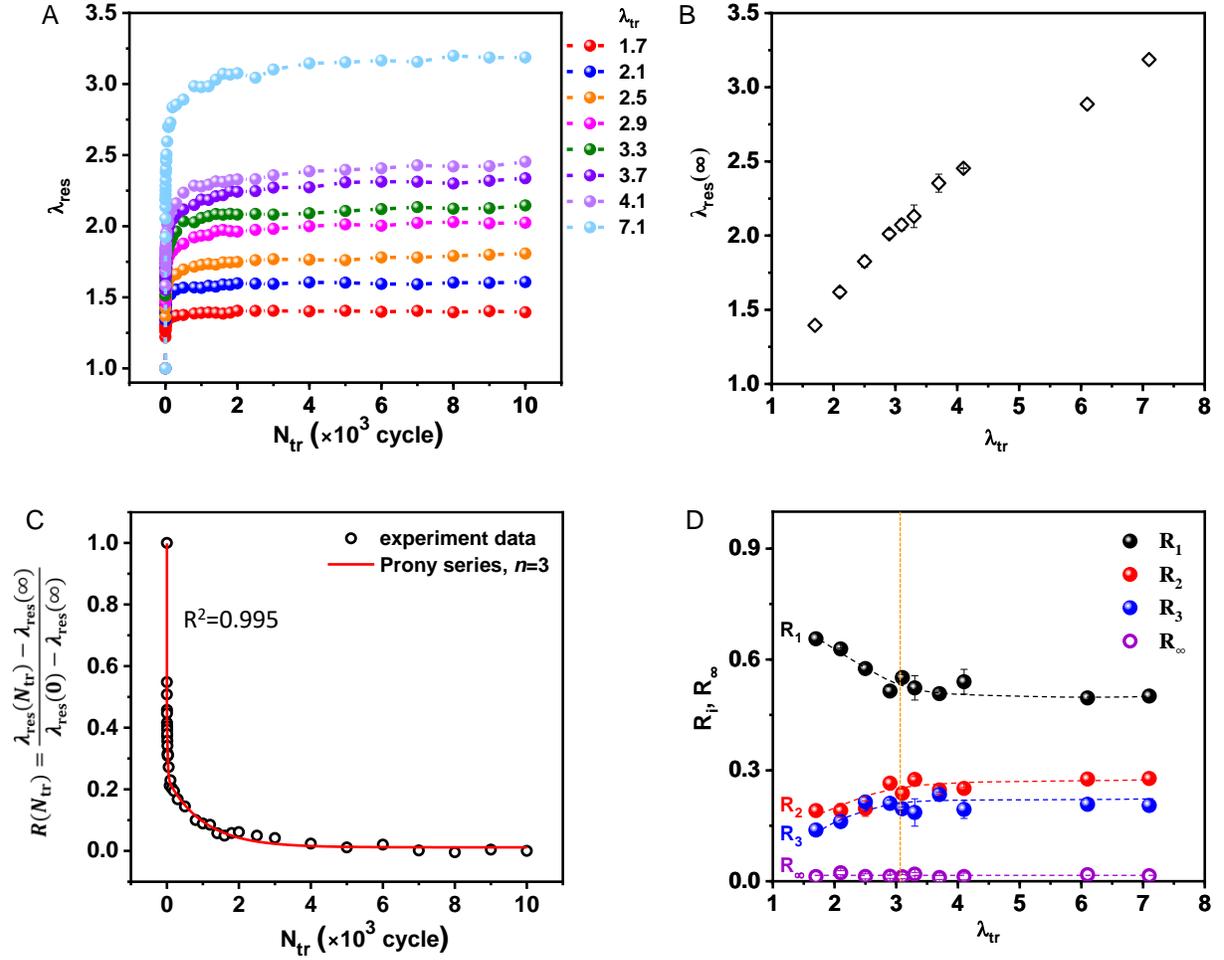
**Fig. S8. Evolution of residual stretch ratio ($\lambda_{res}$) with training cycle $N_{tr}$ of s-PA gel and the Prony series fitting.** (**A**) The residual stretch ratio $\lambda_{res}$ versus $N_{tr}$ for the samples trained at varied $\lambda_{tr}$. (**B**) $\lambda_{res}$ at the steady state of training ($\lambda_{res}(\infty)$) as a function of $\lambda_{tr}$. (**C**) Prony series fitting of normalized $\lambda_{res}$. Here $\lambda_{tr} = 2.9$ is taken as an example. The $\lambda_{res}$ is normalized as $R(N_{tr}) = \dfrac{\lambda_{res}(N_{tr}) - \lambda_{res}(\infty)}{\lambda_{res}(0) - \lambda_{res}(\infty)}$. The $\lambda_{res}(0) = 1$ denotes the $\lambda_{res}$ at the undeformed state. (**D**) The Prony series fitting parameter $R_i$ and $R_\infty$ as a function of $\lambda_{tr}$. The vertical dotted line indicates $\lambda_{affine}$. The dashed lines are a guide for the eyes. The error bar ($\lambda_{tr} = 2.1$ to $3.7$) is SE from at least three measurements.
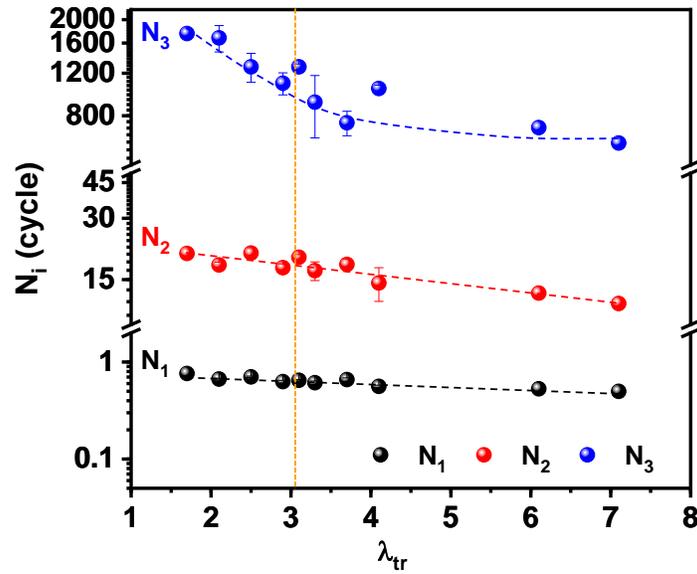
**Fig. S9. The characteristic training cycles of hysteresis energy density $U_{hys}$ of s-PA gel as a function of $\lambda_{tr}$.** The $U_{hys}$ versus $N_{tr}$ profiles are fitted by $U_{hys}(N_{tr}) = U_{hys,\infty} + \sum_{i=1}^{n} U_{hys,i}\, e^{-N_{tr}/N_i}$ , where

$U_{hys}(N_{tr})$ is the $U_{hys}$ (the area between the load and unload curves) at the cycle $N_{tr}$, $U_{hys,\infty}$ is the $U_{hys}$ in the steady state of cyclic loading, $N_i$ are the characteristic training cycles, $U_{hys,i}$ are training strengths, and $n$ is the series order, $n = 3$. The vertical dotted line indicates $\lambda_{affine}$. The error bar ($\lambda_{tr}$ = 2.1 to 3.7) is SE from at least three measurements.

**Section S3. The Prony series fitting of detraining curves**

Detraining experiment is performed by resting the trained sample at 24 °C for varied time $t_{rest}$. As schemed in **fig. S10A**, the trained s-PA gels (trained at $\lambda_{tr}$ for $N_{tr} = 10^4$ cycles) are allowed to rest at a strain-free state for different times $t_{rest}$, then are loaded to $\lambda_{tr}$ to detect the self-recovery efficiency. The longest $t_{rest}$ we tracked are 87 ks for $\lambda_{tr} < 4.1$, and 500 ks for $\lambda_{tr} > 4.1$ (ks means 1000 seconds). We find that the change of mechanical behavior during rest is similar to detraining of muscles, that the temporary memories formed during training process are gradually forgotten during rest. As an example, **Fig. 2C** shows the loading-unloading curves at $t_{rest}$ after the sample being trained at $\lambda_{tr} = 3.7$ for $N_{tr} = 10^4$. The gel self-recovers to its original length, showing no residual strain ($\lambda_{res} = 1$) after resting for $t_{rest} = 25$ ks, while the softening of stress and loss of hysteresis loop still slightly remain after resting for 87 ks. Then, we systematically study the effect of training intensity ($\lambda_{tr}$) on the relaxation dynamics when the training duration is fixed at $N_{tr} = 10^4$. **Fig. S10B** plots the normalized work of extension $W_{ex}(t_{rest})/W_{ex0}$ as a function of $t_{rest}$ for several representative $\lambda_{tr}$, $\lambda_{tr} = 2.9$, 3.7 and 7.1. Note that the $\lambda_{tr} = 2.9$ is smaller than the $\lambda_{affine}$, $\lambda_{tr} = 3.7$ is above the $\lambda_{affine}$, and $\lambda_{tr} = 7.1$ is far beyond the $\lambda_{affine}$. It shows that $W_{ex}(t_{rest})/W_{ex0}$ increases rapidly at the beginning of rest and gradually approaches to 0.9, 0.8 and 0.6 for $\lambda_{tr} = 2.9$, 3.7 and 7.1, respectively, after a long $t_{rest}$. In contrast, the residual stretch ratios $\lambda_{res}(t_{rest})$ of all the trained samples recover to 1 during the rest process in our observation time scale (**fig. S11A**). These detraining curves show that detraining dynamics become slower after suffering a higher training intensity $\lambda_{tr}$.

To clarify the difference in dynamics between the $W_{ex}(t_{rest})$ and $\lambda_{res}(t_{rest})$ during detraining, we also use the Prony series to fit the detraining curves. First, the Prony series is used to fit the normalized $W_{ex}(t_{rest})$, that is $w(t_{rest}) = \dfrac{W_{ex}(t_{rest}) - W_{ex0}}{W_\infty - W_{ex0}}$, where $W_{ex0}$ and $W_\infty$ are the $W_{ex}$ of the first loading and equilibrium $W_{ex}$ in training at $\lambda_{tr}$, respectively. The $w(t_{rest}) = 1$ means no detraining,

and $w(t_{rest}) = 0$ means full recovery during rest. To fit the normalized $w(t_{rest})$, the Prony series is rewritten

$$w(t_{rest}) = w_{\infty} + \sum_{i=1}^{n} w_i e^{-t_{rest}/\tau_{f,i}} \tag{S3}$$

where $w_{\infty}$ is the ratio of irrecoverable part within the maximum observation $t_{rest}$, $w_i$ are detraining strengths of $W_{ex}(t_{rest})$, and $\tau_{f,i}$ are characteristic detraining times, correlated to the forgetting rate of the training effect. Same as the fitting applied in training process, the series order $n = 3$ is used. Taking the gel trained at $\lambda_{tr} = 3.7$ for $N_{tr} = 10^4$ as an example, **fig. S10C** shows that $n = 3$ gives an excellent fitting ($R^2 = 0.999$) for the detraining curve. The characteristic detraining times are $\tau_{f,1} = 42.8$ s, $\tau_{f,2} = 916.4$ s, and $\tau_{f,3} = 12170.9$ s with the detraining parameters $w_1 = 0.11$, $w_2 = 0.17$, $w_3 = 0.42$, and $w_{\infty} = 0.29$.

The detraining curves of $W_{ex}(t_{rest})$ of the gels trained at varied $\lambda_{tr}$ were fitted by **Eq. S3**. The detraining strength $w_i$ is shown in **fig. S10D**, and the characteristic detraining times $\tau_{f,1}$, $\tau_{f,2}$, $\tau_{f,3}$ of $W_{ex}(t_{rest})$ as a function of $\lambda_{tr}$ is shown in **fig. S10E**. The $w_i$ slightly decrease with $\lambda_{tr}$, and have an order of $w_3 > w_2 > w_1$, indicating that the long-term relaxation due to the mesoscale phase networks contributes more than the short-term relaxation due to the transient network. Expectedly, the irrecoverable term $w_{\infty}$ increases with $\lambda_{tr}$ at $\lambda_{affine} < \lambda_{tr} < \lambda_c$, indicating an increased damage of the hard phase network.
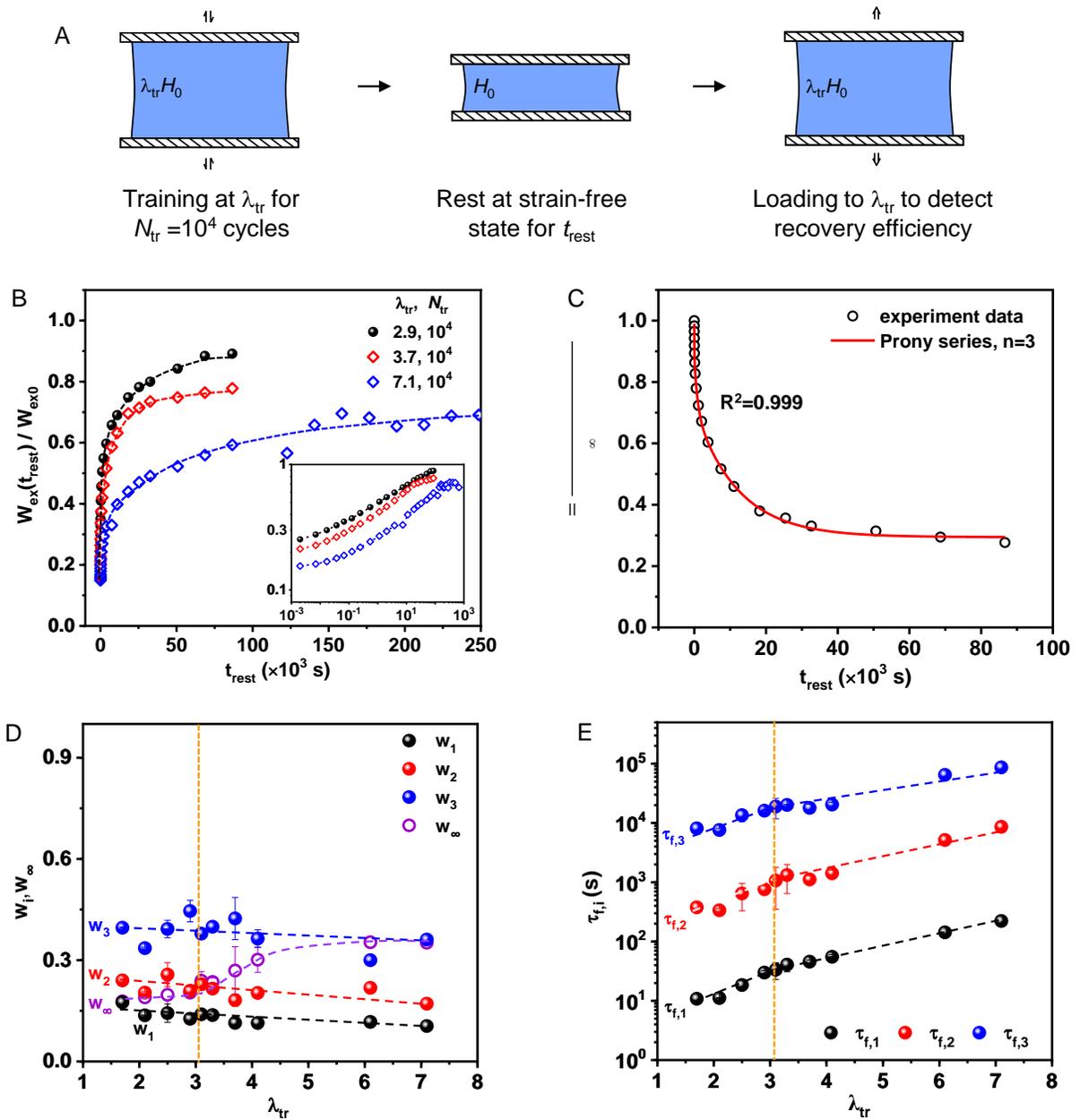
**Fig. S10. Prony series fitting of $W_{ex}(t_{rest})$ versus $t_{rest}$ curves of detraining process for s-PA gel.**
(**A**) Experimental protocol for detraining. After resting for $t_{rest}$, the trained gels (trained at $\lambda_{tr}$ for $N_{tr} = 10^4$ cycles) are reloaded to the corresponding $\lambda_{tr}$ to detect the recovery efficiency. (**B**) Evolution of $W_{ex}(t_{rest})/W_{ex0}$ as a function of rest time $t_{rest}$ after cyclic training under $\lambda_{tr} = 2.9$, 3.7 and 7.1 for $N_{tr} = 10^4$. Inset shows the logarithm plots. (**C**) Prony series fitting of normalized $W_{ex}(t_{rest})$. Here $\lambda_{tr} = 3.7$ for $N_{tr} = 10^4$ is taken as an example. The $W_{ex}(t_{rest})$ is normalized as

$$w(t_{rest}) = \frac{W_{ex}(t_{rest}) - W_{ex0}}{W_{\infty} - W_{ex0}}$$ , where $W_{ex}(t_{rest})$ is the $W_{ex}$ for deforming the trained gel to the

corresponding $\lambda_{tr}$ after resting for $t_{rest}$. $W_{ex0}$ and $W_{\infty}$ are the $W_{ex}$ of the first loading and equilibrium $W_{ex}$ for training at $\lambda_{tr}$, respectively. The $w(t_{rest})$ versus $t_{rest}$ denotes forgetting curve. (**D**) The Prony series parameters $w_i$ and $w_{\infty}$ versus $\lambda_{tr}$. (**E**) The characteristic detraining time (forgetting time) $\tau_{f,1}$, $\tau_{f,2}$, and $\tau_{f,3}$ of $W_{ex}(t_{rest})$ as a function of $\lambda_{tr}$. The vertical dotted line indicates $\lambda_{affine}$. The dashed lines are a guide for the eyes. The error bar ($\lambda_{tr} = 2.1$ to 3.7) is SE from at least three measurements.

Then, the Prony series is used to fit the detraining process of the normalized $\lambda_{res}(t_{rest})$, which is

$R_f(t_{rest}) = \dfrac{\lambda_{res}(t_{rest})}{\lambda_{res}(\infty)}$. Now the Prony series is rewritten as

$$R_f(t_{rest}) = \sum_{i=1}^{n} R_{f,i} e^{-t_{rest}/\tau_{f,i}} \tag{S4}$$

Note that, due to all the $\lambda_{res}(t_{rest})$ can recover to pristine state, there is no infinity term in **Eq. S4**.

$R_{f,i}$ are the detraining strengths of $\lambda_{res}(t_{rest})$, and $\tau_{f,i}$ are the characteristic detraining time of $\lambda_{res}(t_{rest})$.

**Figure S11B** shows one example of the fitting result of normalized residual stretch ratio $R_f(t_{rest})$ at

$\lambda_{tr} = 3.7$ using $n = 3$. The good fitting ($R^2 = 0.994$) gives characteristic detraining times $\tau_{f,1} = 1$ s,

$\tau_{f,2} = 119.9$ s, and $\tau_{f,3} = 4630.9$ s with the detraining parameters $R_{f,1} = 0.34$, $R_{f,2} = 0.28$, $R_{f,3} = 0.36$.

The detraining curves of $\lambda_{res}(t_{rest})$ of the gel trained at varied $\lambda_{tr}$ were fitted by **Eq. S4**. The

detraining strengths $R_{f,i}$ are shown in **fig. S11C** and the characteristic detraining times $\tau_{f,1}$, $\tau_{f,2}$, $\tau_{f,3}$

of $\lambda_{res}(t_{rest})$ as a function of $\lambda_{tr}$ is shown in **fig. S11D**. The three fitting parameters $R_{f,i}$ have a similar

value (around 0.3), and depend little on the training $\lambda_{tr}$. This indicates that the structures with varied

length scales almost contribute equal to the detraining strengths of $\lambda_{res}$.
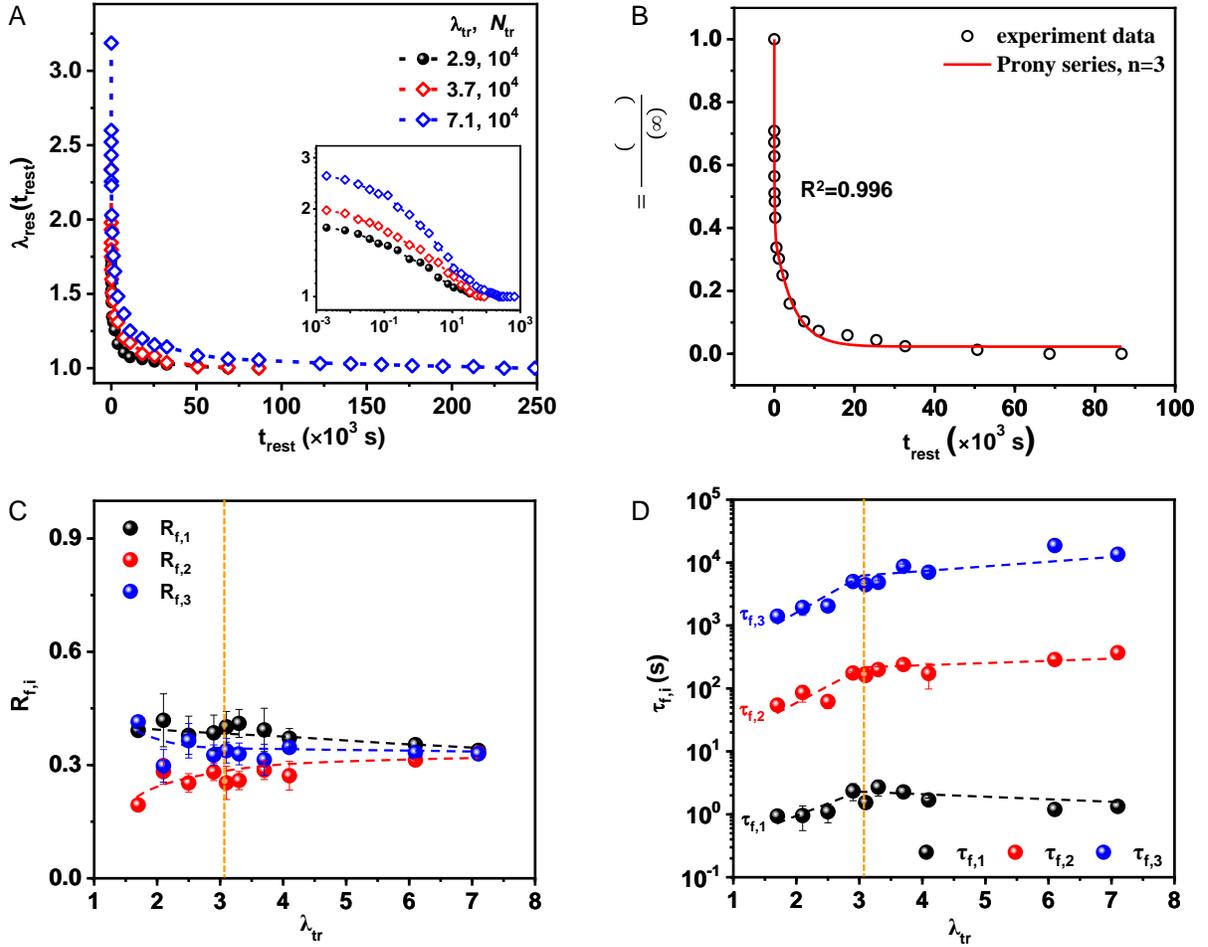
**Fig. S11. Prony series fitting of $\lambda_{res}(t_{rest})$ versus $t_{rest}$ curves of detraining process for s-PA gel.**
(**A**) Evolution of $\lambda_{res}(t_{rest})$ as a function of rest time $t_{rest}$ after cyclic training under $\lambda_{tr} = 2.9$, 3.7 and 7.1 for $N_{tr} = 10^4$. Inset shows the logarithm plots. (**B**) Prony series fitting of normalized $\lambda_{res}(t_{rest})$.

Here $\lambda_{tr} = 3.7$ for $N_{tr} = 10^4$ is taken as an example. The $\lambda_{res}(t_{rest})$ is normalized as $R_f(t_{rest}) = \dfrac{\lambda_{res}(t_{rest})}{\lambda_{res}(\infty)}$,

where $\lambda_{res}(t_{rest})$ is the $\lambda_{res}$ at rest time $t_{rest}$, and $\lambda_{res}(\infty)$ is the equilibrium $\lambda_{res}$ in the training process.
(**C**) The Prony series parameters $R_{f,i}$ as a function of $\lambda_{tr}$. (**D**) The characteristic detraining time
(forgetting time) $\tau_{f,1}$, $\tau_{f,2}$, and $\tau_{f,3}$ of $\lambda_{res}(t_{rest})$ as a function of $\lambda_{tr}$. The vertical dotted line indicates
$\lambda_{affine}$. The dashed lines are a guide for the eyes. The error bar ($\lambda_{tr} = 2.1$ to 3.7) is SE from at least
three measurements.
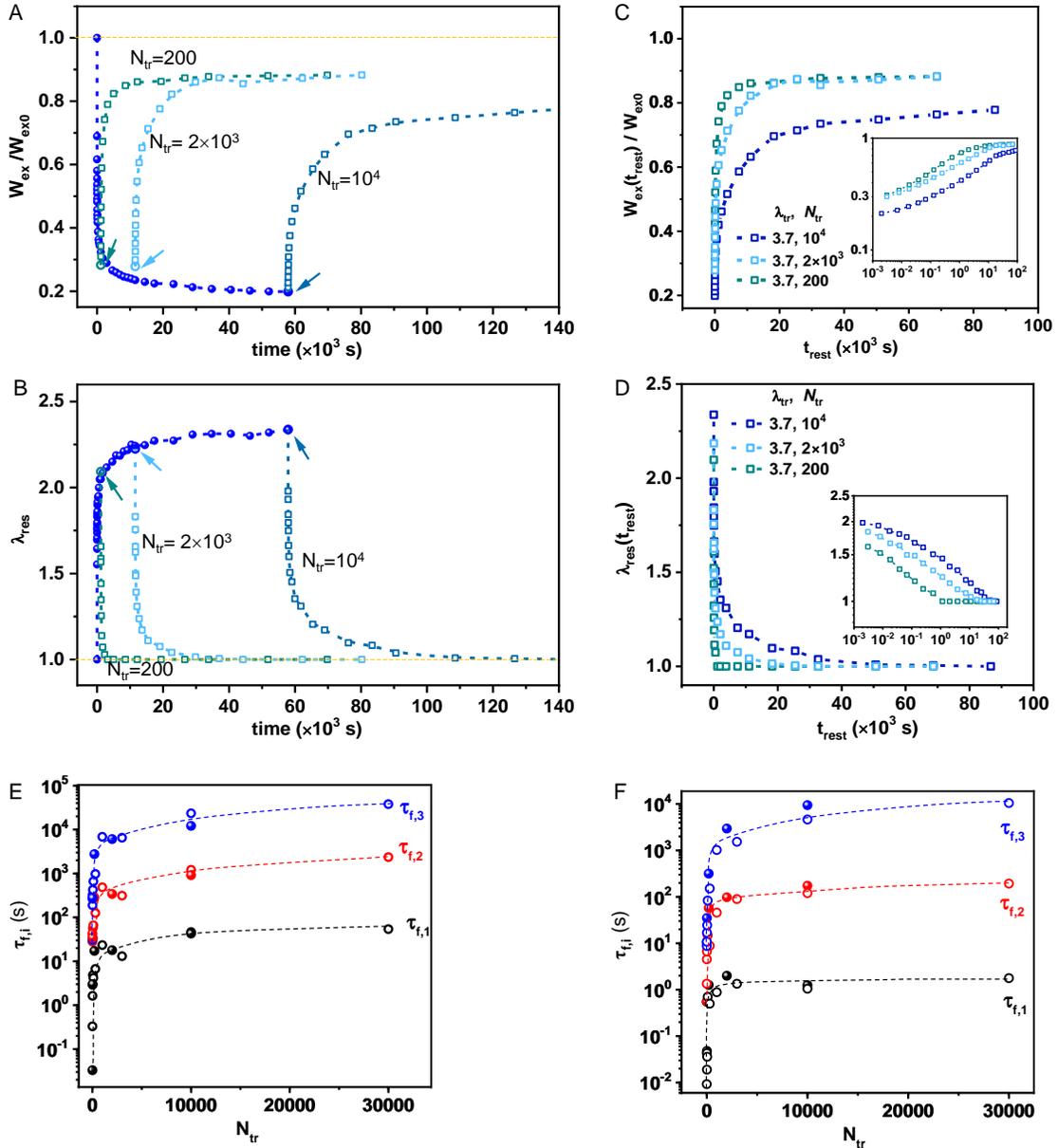
**Fig. S12. Effect of training duration $N_{tr}$ on detraining dynamics of s-PA gel. (A)** The $W_{ex}/W_{ex0}$ and **(B)** the residual stretch ratio $\lambda_{res}$ in cyclic training and detraining as a function of time (both training and rest time). Training at fixed $\lambda_{tr} = 3.7$ for $N_{tr} = 200, 2000, 10^4$ are taken as examples. Cyclic training is plotted by spheres and the detraining process is plotted by open symbols. The arrows indicate the points at which the samples are allowed to rest, and the corresponding $N_{tr}$ are shown next to each detraining curve. **(C)** Evolution of $W_{ex}(t_{rest})/W_{ex0}$ as a function of rest time $t_{rest}$. The data is extracted from (A). **(D)** Evolution of $\lambda_{res}(t_{rest})$ as a function of rest time $t_{rest}$. The data is extracted from (B). **(E)** The characteristic detraining time (forgetting time) $\tau_{f,1}$, $\tau_{f,2}$, and $\tau_{f,3}$ of $W_{ex}(t_{rest})$ versus $N_{tr}$. **Eq. S3** is used for fitting the $W_{ex}(t_{rest})$ curves of detraining. **(F)** The characteristic detraining time (forgetting time) $\tau_{f,1}$, $\tau_{f,2}$, and $\tau_{f,3}$ of $\lambda_{res}(t_{rest})$ versus $N_{tr}$. **Eq. S4** is used for fitting the $\lambda_{res}(t_{rest})$ curves of detraining. In **(E)** and **(F)**, the circles denote training at $\lambda_{tr} = 2.9$ for varied $N_{tr}$ and the spheres denote training at $\lambda_{tr} = 3.7$ for varied $N_{tr}$. The characteristic detraining times $\tau_{f,1}$, $\tau_{f,2}$, and $\tau_{f,3}$ of both $W_{ex}(t_{rest})$ and $\lambda_{res}(t_{rest})$ indicate that $N_{tr} \geq 1000$ is required for saturated training.
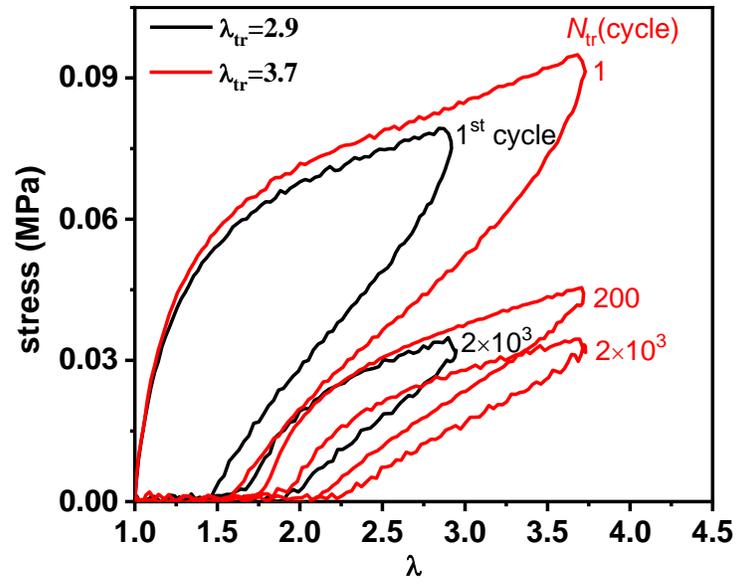
**Fig. S13. Loading-unloading curves of the unnotched s-PA samples during cyclic training under $\lambda_{tr}$ = 2.9 ($< \lambda_{affine}$) and $\lambda_{tr}$ = 3.7 ($> \lambda_{affine}$).**
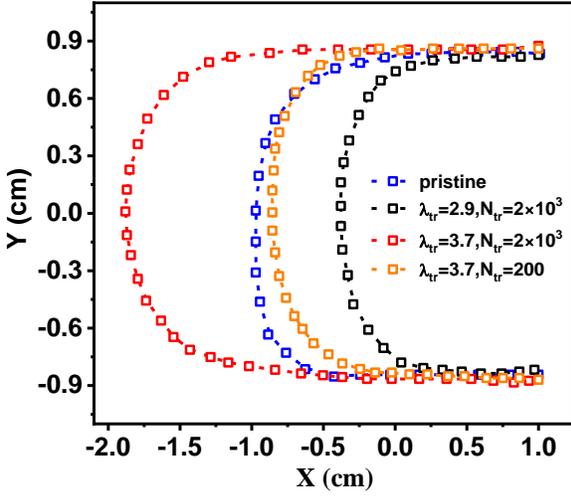
| Sample | $N_{fatigue}$ (cycle) | Radius of curvature at crack tip (cm) |
|---|---|---|
| pristine | $9\times10^3$ | 1.83 |
| $\lambda_{tr} = 2.9$, $N_{tr} = 2\times10^3$ | $9\times10^3$ | 1.80 |
| $\lambda_{tr} = 3.7$, $N_{tr} = 2\times10^3$ | $1.8\times10^3$ | 0.77 |
| $\lambda_{tr} = 3.7$, $N_{tr} = 200$ | $9\times10^3$ | 1.56 |

**Fig. S14. Crack tip profiles of s-PA gels during fatigue test at $\lambda_{fatigue} = 2.9$ after trained at varied conditions and the radius of curvature at the crack tip ($R$).** The data is extracted from **Fig. 4B**. $X = 0$ denotes the position of pre-cut perpendicular to loading direction, and $Y = 0$ denotes the center of crack along the loading direction. The radius of curvature at the crack tip $R$ is obtained at $Y \approx 0$ by $R = \left| \frac{\left(1+X'^2\right)^{3/2}}{X''} \right|$, where $X' = \frac{dX}{dY}$ and $X'' = \frac{d^2X}{dY^2}$.

## Section S4. Direct fatigue test

For the direct fatigue test, the pre-notched s-PA gel with the pure shear geometry (inset of **fig. 15A**) was used. Consecutive cyclic loading without interval between cycles was performed at preset $\lambda_{fatigue}$. The crack propagation with cycles is recorded as $c$. Self-training effect is observed at $\lambda_{fatigue} \leq \lambda_{tran}$ while overtraining happens at $\lambda_{fatigue} > \lambda_{tran}$. The former shows that the stress concentration gradually weakens with cycle number $N_{fatigue}$ (**fig. S15B**), whereas the latter shows that the crack tip always has severe stress concentration (**fig. S15C**). The $\lambda_{tran} = 3.1$ ($\approx \lambda_{affine}$) is the slow-to-fast crack propagation transition stretch ratio in the direct fatigue test as indicated in our previous work (*49*).
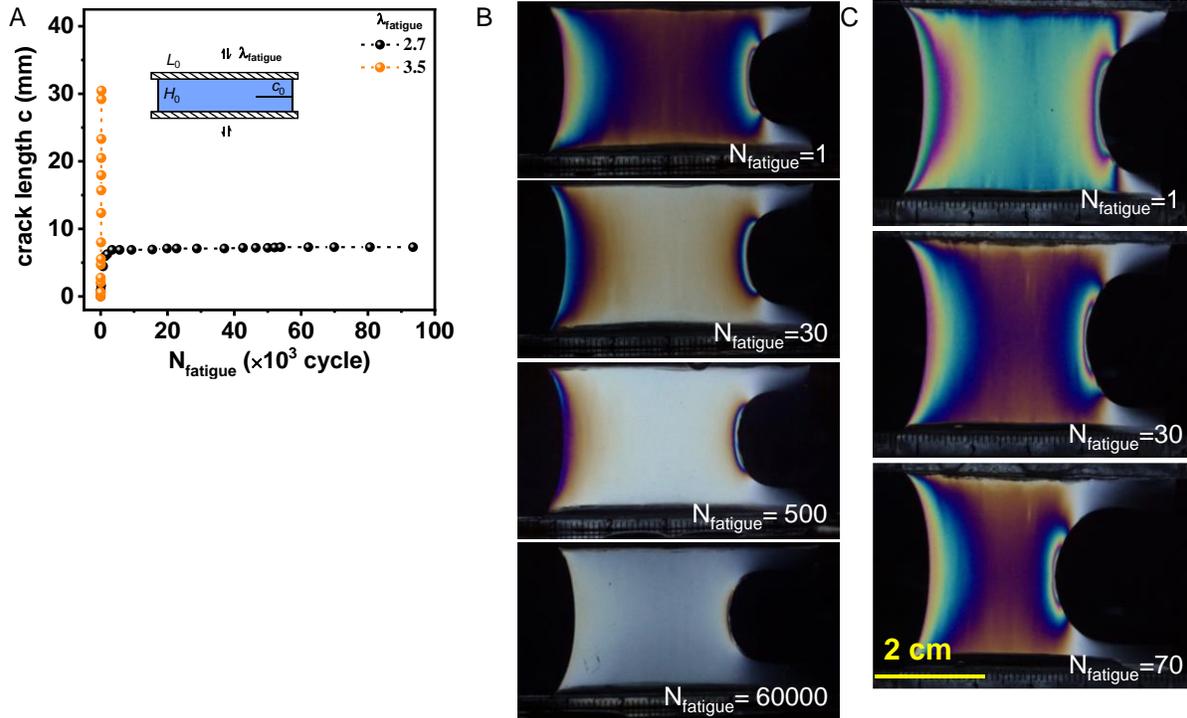


**Fig. S15. Self-training and overtraining effect in direct fatigue test using pre-notched s-PA samples.** (**A**) Fatigue behavior of the pristine notched gel (inset, $L_0 = 50$ mm, $H_0 = 10$ mm, and $c_0 = 10$ mm) at $\lambda_{fatigue} = 2.7 < \lambda_{tran}$ and $\lambda_{fatigue} = 3.5 > \lambda_{tran}$. Typical evolution of birefringence images with cycle number $N_{fatigue}$ at $\lambda_{fatigue} = 2.7$ (**B**) and $\lambda_{fatigue} = 3.5$ (**C**).
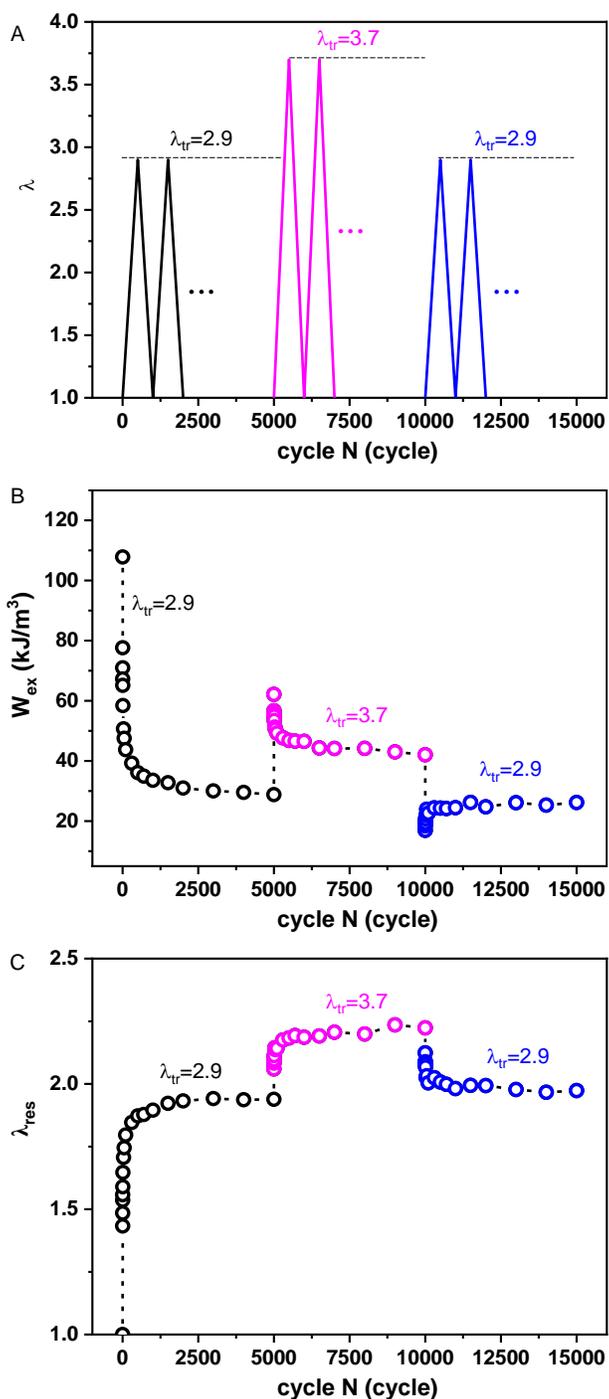
**Fig. S16. Mechanical adaptation of s-PA gel under stepwise cyclic stretching.** (**A**) Experiment proposal for training. One piece of s-PA gel undergoes the following training protocol. Initially, it is subjected to cyclic loading at a preset $\lambda_{tr} = 2.9$ for $N_{tr} = 5000$ cycles. Subsequently, the $\lambda_{tr}$ is increased to $\lambda_{tr} = 3.7$ and the sample undergoes an additional $N_{tr} = 5000$ cycles. Finally, the $\lambda_{tr}$ is reduced back $\lambda_{tr} = 2.9$ for cyclic training. The corresponding (**B**) strain energy density obtained from the loading curves ($W_{ex}$) and (**C**) the residual stretch ratio ($\lambda_{res}$). We can see that both the $W_{ex}$ and $\lambda_{res}$ can rapidly adapt to the mechanical training. Notably, at the two $\lambda_{tr} = 2.9$, the $W_{ex}$ and $\lambda_{res}$ exhibit similar values in the steady state, despite having different training histories.

# REFERENCES

1. M. P. McHugh, C. H. Cosgrave, To stretch or not to stretch: The role of stretching in injury prevention and performance. *Scand. J. Med. Sci. Sports* **20**, 169–181 (2010).

2. I. Mujika, S. Padilla, Detraining: Loss of training-induced physiological and performance adaptations. Part II: Long term insufficient training stimulus. *Sports Med.* **30**, 145–154 (2000).

3. I. Mujika, S. Padilla, Detraining: Loss of training-induced physiological and performance adaptations. Part I: Short term insufficient training stimulus. *Sports Med.* **30**, 79–87 (2000).

4. N. Matos, R. J. Winsley, Trainability of young athletes and overtraining. *J. Sports Sci. Med.* **6**, 353–367 (2007).

5. L. L. Smith, Tissue trauma: The underlying cause of overtraining syndrome? *J. Strength Cond. Res.* **18**, 185–193 (2004).

6. T. Nonoyama, J. P. Gong, Tough double network hydrogel and its biomedical applications. *Annu. Rev. Chem. Biomol. Eng.* **12**, 393–410 (2021).

7. T. Matsuda, Kawakami, R., Namba, R., Nakajima, T., & Gong, J. P., Mechanoresponsive self-growing hydrogels inspired by muscle training. *Science* **363**, 504–508 (2019).

8. Z. J. Wang, J. Jiang, Q. Mu, S. Maeda, T. Nakajima, J. P. Gong, Azo-crosslinked double-network hydrogels enabling highly efficient mechanoradical generation. *J. Am. Chem. Soc.* **144**, 3154–3161 (2022).

9. S. Lin, J. Liu, X. Liu, X. Zhao, Muscle-like fatigue-resistant hydrogels by mechanical training. *Proc. Natl. Acad. Sci. U.S.A.* **116**, 10244–10249 (2019).

10. J. N. Jin, X. R. Yang, Y. F. Wang, L. M. Zhao, L. P. Yang, L. Huang, W. Jiang, Mechanical training enabled reinforcement of polyrotaxane-containing hydrogel. *Angew. Chem. Int. Ed. Engl.* **62**, e202218313 (2023).

11. Z. Lei, W. Gao, W. Zhu, P. Wu, Anti-fatigue and highly conductive thermocells for continuous electricity generation. *Adv. Funct. Mater.* **32**, 2201021 (2022).

12. Z. Wang, J. Tang, R. Bai, W. Zhang, T. Lian, T. Lu, T. Wang, A phenomenological model for shakedown of tough hydrogels under cyclic loads. *J. Appl. Mech.* **85**, 091005 (2018).

13. Y. Zhou, J. Hu, P. Zhao, W. Zhang, Z. Suo, T. Lu, Flaw-sensitivity of a tough hydrogel under monotonic and cyclic loads. *J. Mech. Phys. Solids* **153**, 104483 (2021).

14. R. Bai, J. Yang, Z. Suo, Fatigue of hydrogels. *Eur. J. Mech. A Solids* **74**, 337–370 (2019).

15. J. Tang, J. Li, J. J. Vlassak, Z. Suo, Fatigue fracture of hydrogels. *Extreme Mech. Lett.* **10**, 24–31 (2017).

16. W. Zhang, J. Hu, H. Yang, Z. Suo, T. Lu, Fatigue-resistant adhesion II: Swell tolerance. *Extreme Mech. Lett.* **43**, 101182 (2021).

17. C. Xiang, Z. Wang, C. Yang, X. Yao, Y. Wang, Z. Suo, Stretchable and fatigue-resistant materials. *Mater. Today* **34**, 7–16 (2020).

18. E. Zhang, R. Bai, X. P. Morelle, Z. Suo, Fatigue fracture of nearly elastic hydrogels. *Soft Matter* **14**, 3563–3571 (2018).

19. J. Ni, S. Lin, Z. Qin, D. Veysset, X. Liu, Y. Sun, A. J. Hsieh, R. Radovitzky, K. A. Nelson, X. Zhao, Strong fatigue-resistant nanofibrous hydrogels inspired by lobster underbelly. *Matter* **4**, 1919–1934 (2021).

20. X. Liang, G. Chen, S. Lin, J. Zhang, L. Wang, P. Zhang, Y. Lan, J. Liu, Bioinspired 2D isotropically fatigue-resistant hydrogels. *Adv. Mater.* **34**, e2107106 (2022).

21. M. Hua, S. Wu, Y. Ma, Y. Zhao, Z. Chen, I. Frenkel, J. Strzalka, H. Zhou, X. Zhu, X. He, Strong tough hydrogels via the synergy of freeze-casting and salting out. *Nature* **590**, 594–599 (2021).

22. S. Lin, X. Liu, J. Liu, H. Yuk, H.-C. Loh, G. A. Parada, C. Settens, J. Song, A. Masic, G. H. McKinley, Anti-fatigue-fracture hydrogels. *Sci. Adv.* **5**, eaau8528 (2019).

23. G. Zhang, J. Kim, S. Hassan, Z. Suo, Self-assembled nanocomposites of high water content and load-bearing capacity. *Proc. Natl. Acad. Sci. U.S.A.* **119**, e2203962119 (2022).

24. J.-Y. Sun, X. Zhao, W. R. Illeperuma, O. Chaudhuri, K. H. Oh, D. J. Mooney, J. J. Vlassak, Z. Suo, Highly stretchable and tough hydrogels. *Nature* **489**, 133–136 (2012).

25. J. Li, Z. Suo, J. J. Vlassak, Stiff, strong, and tough hydrogels with good chemical stability. *J. Mater. Chem. B* **2**, 6708–6713 (2014).

26. R. Bai, J. Yang, X. P. Morelle, C. Yang, Z. Suo, Fatigue fracture of self-recovery hydrogels. *ACS Macro Lett.* **7**, 312–317 (2018).

27. P. Lin, S. Ma, X. Wang, F. Zhou, Molecularly engineered dual-crosslinked hydrogel with ultrahigh mechanical strength, toughness, and good self-recovery. *Adv. Mater.* **27**, 2054–2059 (2015).

28. H. C. Yu, S. Y. Zheng, L. Fang, Z. Ying, M. Du, J. Wang, K. F. Ren, Z. L. Wu, Q. Zheng, Reversibly transforming a highly swollen polyelectrolyte hydrogel to an extremely tough one and its application as a tubular grasper. *Adv. Mater.* **32**, e2005171 (2020).

29. H. Sun, S. Li, K. Li, Y. Liu, C. Tang, Z. Liu, L. Zhu, J. Yang, G. Qin, Q. Chen, Tough and self-healable carrageenan-based double network microgels enhanced physical hydrogels for strain sensor. *J. Polym. Sci.* **60**, 2720–2732 (2021).

30. Q. Chen, L. Zhu, C. Zhao, Q. Wang, J. Zheng, A robust, one-pot synthesis of highly mechanical and recoverable double network hydrogels using thermoreversible sol-gel polysaccharide. *Adv. Mater.* **25**, 4171–4176 (2013).

31. R. Long, K. Mayumi, C. Creton, T. Narita, C.-Y. Hui, Time dependent behavior of a dual cross-link self-healing gel: Theory and experiments. *Macromolecules* **47**, 7243–7250 (2014).

32. K. Mayumi, J. Guo, T. Narita, C. Y. Hui, C. Creton, Fracture of dual crosslink gels with permanent and transient crosslinks. *Extreme Mech. Lett.* **6**, 52–59 (2016).

33. K. Mayumi, A. Marcellan, G. Ducouret, C. Creton, T. Narita, Stress–strain relationship of highly stretchable dual cross-link gels: Separability of strain and time effect. *ACS Macro Lett.* **2**, 1065–1068 (2013).

34. M. Rodin, J. Li, D. Kuckling, Dually cross-linked single networks: Structures and applications. *Chem. Soc. Rev.* **50**, 8147–8177 (2021).

35. T. Narita, K. Mayumi, G. Ducouret, P. Hébraud, Viscoelastic properties of poly(vinyl alcohol) hydrogels having permanent and transient cross-links studied by microrheology, classical rheometry, and dynamic light scattering. *Macromolecules* **46**, 4174–4183 (2013).

36. V. Yesilyurt, M. J. Webber, E. A. Appel, C. Godwin, R. Langer, D. G. Anderson, Injectable self-healing glucose-responsive hydrogels with pH-regulated mechanical properties. *Adv. Mater.* **28**, 86–91 (2016).

37. M. Ohira, T. Katashima, M. Naito, D. Aoki, Y. Yoshikawa, H. Iwase, S. I. Takata, K. Miyata, U. I. Chung, T. Sakai, M. Shibayama, X. Li, Star-polymer-DNA gels showing highly predictable and tunable mechanical responses. *Adv. Mater.* **34**, e2108818 (2022).

38. V. Yesilyurt, A. M. Ayoob, E. A. Appel, J. T. Borenstein, R. Langer, D. G. Anderson, Mixed reversible covalent crosslink kinetics enable precise, hierarchical mechanical tuning of hydrogel networks. *Adv. Mater.* **29**, 1605947 (2017).

39. M. Zhang, D. Xu, X. Yan, J. Chen, S. Dong, B. Zheng, F. Huang, Self-healing supramolecular gels formed by crown ether based host-guest interactions. *Angew. Chem. Int. Ed. Engl.* **51**, 7011–7015 (2012).

40. A. Harada, Y. Takashima, A. Hashidzume, H. Yamaguchi, Supramolecular polymers and materials formed by host-guest interactions. *Bull. Chem. Soc. Jpn.* **94**, 2381–2389 (2021).

41. M. Nakahata, Y. Takashima, A. Harada, Highly flexible, tough, and self-healing supramolecular polymeric materials using host-guest interaction. *Macromol. Rapid Commun.* **37**, 86–92 (2016).

42. R. S. Staron, M. J. Leonardi, D. L. Karapondo, E. S. Malicky, J. E. Falkel, F. C. Hagerman, R. S. Hikida, Strength and skeletal muscle adaptations in heavy-resistance-trained women after detraining and retraining. *J. Appl. Physiol.* **70**, 631–640 (1991).

43. K. M. Wisdom, S. L. Delp, E. Kuhl, Use it or lose it: Multiscale skeletal muscle adaptation to mechanical stimuli. *Biomech. Model. Mechanobiol.* **14**, 195–215 (2015).

44. T. L. Sun, T. Kurokawa, S. Kuroda, A. B. Ihsan, T. Akasaki, K. Sato, M. A. Haque, T. Nakajima, J. P. Gong, Physical hydrogels composed of polyampholytes demonstrate high toughness and viscoelasticity. *Nat. Mater.* **12**, 932–937 (2013).

45. X. Li, F. Luo, T. L. Sun, K. Cui, R. Watanabe, T. Nakajima, J. P. Gong, Effect of salt on dynamic mechanical behaviors of polyampholyte hydrogels. *Macromolecules* **56**, 535–544 (2023).

46. K. Cui, J. P. Gong, How double dynamics affects the large deformation and fracture behaviors of soft materials. *J. Rheol.* **66**, 1093–1111 (2022).

47. X. Li, J. P. Gong, Role of dynamic bonds on fatigue threshold of tough hydrogels. *Proc. Natl. Acad. Sci. U.S.A.* **119**, e2200678119 (2022).

48. A. Eisenberg, B. Hird, R. Moore, A new multiplet-cluster model for the morphology of random ionomers. *Macromolecules* **23**, 4098–4107 (1990).

49. X. Li, K. Cui, T. L. Sun, L. Meng, C. Yu, L. Li, C. Creton, T. Kurokawa, J. P. Gong, Mesoscale bicontinuous networks in self-healing hydrogels delay fatigue fracture. *Proc. Natl. Acad. Sci. U.S.A.* **117**, 7606–7612 (2020).

50. X. Li, K. Cui, T. Kurokawa, Y. N. Ye, T. L. Sun, C. Yu, C. Creton, J. P. Gong, Effect of mesoscale phase contrast on fatigue-delaying behavior of self-healing hydrogels. *Sci. Adv.* **7**, eabe8210 (2021).

51. K. Cui, T. L. Sun, X. Liang, K. Nakajima, Y. N. Ye, L. Chen, T. Kurokawa, J. P. Gong, Multiscale energy dissipation mechanism in tough and self-healing hydrogels. *Phys. Rev. Lett.* **121**, 185501 (2018).

52. K. Häkkinen, M. Alen, M. Kallinen, R. Newton, W. Kraemer, Neuromuscular adaptation during prolonged strength training, detraining and re-strength-training in middle-aged and elderly people. *Eur. J. Appl. Physiol.* **83**, 51–62 (2000).

53. G. Gavronski, A. Veraksits, E. Vasar, J. Maaroos, Evaluation of viscoelastic parameters of the skeletal muscles in junior triathletes. *Physiol. Meas.* **28**, 625–637 (2007).

54. R. Bai, Q. Yang, J. Tang, X. P. Morelle, J. Vlassak, Z. Suo, Fatigue fracture of tough hydrogels. *Extreme Mech. Lett.* **15**, 91–96 (2017).

55. L. Chen, T. L. Sun, K. Cui, D. R. King, T. Kurokawa, Y. Saruwatari, J. P. Gong, Facile synthesis of novel elastomers with tunable dynamics for toughness, self-healing and adhesion. *J. Mater. Chem. A* **7**, 17334–17344 (2019).

56. J. P. Gong, Why are double network hydrogels so tough?. *Soft Matter* **6**, 2583 (2010).

57. T. Nakajima, H. Furukawa, Y. Tanaka, T. Kurokawa, Y. Osada, J. P. Gong, True chemical structure of double network hydrogels. *Macromolecules* **42**, 2184–2189 (2009).

58. J. P. Gong, Y. Katsuyama, T. Kurokawa, Y. Osada, Double-network hydrogels with extremely high mechanical strength. *Adv. Mater.* **15**, 1155–1158 (2003).

59. A. J. Cunanan, B. H. DeWeese, J. P. Wagle, K. M. Carroll, R. Sausaman, W. G. Hornsby, G. G. Haff, N. T. Triplett, K. C. Pierce, M. H. Stone, The general adaptation syndrome: A foundation for the concept of periodization. *Sports Med.* **48**, 787–797 (2018).

60. A. Bandyopadhyay, I. Bhattacharjee, P. Sousana, Physiological perspective of endurance overtraining—A comprehensive update. *Al Ameen J. Med. Sci.* **5**, 7–20 (2012).

61. B. R. Freedman, J. J. Sarver, M. R. Buckley, P. B. Voleti, L. J. Soslowsky, Biomechanical and structural response of healing Achilles tendon to fatigue loading following acute injury. *J. Biomech.* **47**, 2028–2034 (2014).

62. G. Lake, A. Thomas, The strength of highly elastic materials. *Proc. R. Soc. Lond. A Math. Phys. Sci.* **300**, 108–119 (1967).

63. S. Mzabi, D. Berghezan, S. Roux, F. Hild, C. Creton, A critical local energy release rate criterion for fatigue fracture of elastomers. *J Polym. Sci. B* **49**, 1518–1524 (2011).

64. A. B. Ihsan, T. L. Sun, T. Kurokawa, S. N. Karobi, T. Nakajima, T. Nonoyama, C. K. Roy, F. Luo, J. P. Gong, Self-healing behaviors of tough polyampholyte hydrogels. *Macromolecules* **49**, 4245–4252 (2016).

65. A. B. Ihsan, T. L. Sun, S. Kuroda, M. A. Haque, T. Kurokawa, T. Nakajima, J. P. Gong, A phase diagram of neutral polyampholyte–From solution to tough hydrogel. *J. Mater. Chem. B* **1**, 4555–4562 (2013).

66. K. Cui, Y. N. Ye, T. L. Sun, C. Yu, X. Li, T. Kurokawa, J. P. Gong, Phase separation behavior in tough and self-healing polyampholyte hydrogels. *Macromolecules* **53**, 5116–5126 (2020).

67. F. Luo, T. L. Sun, T. Nakajima, T. Kurokawa, Y. Zhao, A. B. Ihsan, H. L. Guo, X. F. Li, J. P. Gong, Crack blunting and advancing behaviors of tough and self-healing polyampholyte hydrogel. *Macromolecules* **47**, 6037–6046 (2014).

68. H. F. Brinson, L. C. Brinson, in *Polymer Engineering Science and Viscoelasticity* (Springer, 2008), pp. 99–157.

69. S. Park, R. Schapery, Methods of interconversion between linear viscoelastic material functions. Part I—A numerical method based on Prony series. *Int. J. Solids Struct.* **36**, 1653–1675 (1999).

70. E. M. Zanetti, M. Perrini, C. Bignardi, A. L. Audenino, Bladder tissue passive response to monotonic and cyclic loading. *Biorheology* **49**, 49–63 (2012).

71. C.-Y. Hui, B. Zhu, R. Long, Steady state crack growth in viscoelastic solids: A comparative study. *J. Mech. Phys. Solids* **159**, 104748 (2022).

72. J. Guo, M. Liu, A. T. Zehnder, J. Zhao, T. Narita, C. Creton, C.-Y. Hui, Fracture mechanics of a self-healing hydrogel with covalent and physical crosslinks: A numerical study. *J. Mech. Phys. Solids* **120**, 79–95 (2018).

73. M. M. Fitzgerald, K. Bootsma, J. A. Berberich, J. L. Sparks, Tunable stress relaxation behavior of an alginate-polyacrylamide hydrogel: Comparison with muscle tissue. *Biomacromolecules* **16**, 1497–1505 (2015).